DOI: 10.13009/EUCASS2019-260

Combustion characteristics of model composite propellants containing boron and its compounds

Glotov O. G., Yagodnikov D. A.**, Kiskin A. B.***, Surodin G. S.*****

** Voevodsky Institute of Chemical Kinetics and Combustion, Siberian Branch of the Russian Academy of Sciences, 630090, Institutskaya str., 3, Novosibirsk, Russia*

Novosibirsk State Technical University, 630073, Karl Marx ave., 20, Novosibirsk, Russia

glotov@kinetics.nsc.ru

*** Bauman Moscow State Technical University,*

105005, 2nd Baumanskaya str., 5/1, Moscow, Russia

daj@bmstu.ru

**** Voevodsky Institute of Chemical Kinetics and Combustion, Siberian Branch of the Russian Academy of Sciences, 630090, Institutskaya str., 3, Novosibirsk, Russia*

kiskin@kinetics.nsc.ru

***** Voevodsky Institute of Chemical Kinetics and Combustion, Siberian Branch of the Russian Academy of Sciences, 630090, Institutskaya str., 3, Novosibirsk, Russia*

surodin@kinetics.nsc.ru

Abstract

The sampling technique was used to investigate the model composite propellants based on ammonium perchlorate, energetic binder, and boron-containing “metal” fuel. The nominal content of fuel was constantly about 40 %. Boron, aluminum diboride, aluminum dodecaboride, Al+B mechanical mixtures, and boron carbide were employed as a fuel. Data on the burning rate at pressures of 1.2 MPa and 2.5 MPa are presented along with the characteristics of condensed combustion products particles, extinguished at a distance of ~25 mm from the burning surface. The promising propellant formulations are specified for future investigations.

1. Introduction

One of the ways to develop solid propellant rocket motors is to improve the formulation of composite propellants. The synthesis of novel high-energetic materials, the search and the use of more efficient oxidizers and fuels ensure progress in this area [1]. At present, the metal Al fuel, in the form of micrometer particles, is widely used in propellants for the devices, creating jet thrusts [2] [3]. Boron is investigated as propellant ingredient [4] [5] [6] [7] too. Mg, Al+Mg alloys, Li are also investigated, including in the form of aero suspension and aerogels [8] [9] [10]. The possibility is investigated to use Ti, Zr, a series of hydrides [11] [12] [13], as well as combustible metals (primarily Al) in the form of nano-sized particles [14] [15] [16]. The combustion heat, Q, of metal fuel has a considerable effect on propellant energy characteristics. The Q value of boron, calculated per unit of metal mass, exceeds those of the above-mentioned fuels. However, boron is difficult to burn out with high combustion completeness due to the specific combination of the physico-chemical properties of boron and its oxide. In addition, the oxidation of boron needs much more oxygen than the oxidation of other fuels; boron is poorly compatible with other propellant components and costs much. Being the first candidate for application in the systems using outboard oxidizers [4] [5] [17] [18] [19], boron is not the only candidate because of the afore-mentioned disadvantages. Thus, already in the 1970s, aluminum borides were proposed for application [19] and the studies on boron carbide combustion were initiated [20]. The propellants, based on combined fuels (e. g., B+Mg, B+Al) and boron compounds, the optimization of gaseous oxidizer injection [21] [22] and other potentialities were studied in order to increase the boron combustion completeness. Therefore, it is highly essential to extract basic information on the behavior of boron-containing fuels in a combustion wave of composite propellants and to compare formulations with various fuels. In particular, of peculiar interest are the parameters of the particles, leaving the burning surface, as they set the initial conditions of particle evolution upon their motion along the path of the motor. These particles are usually named “the primary combustion products” [23]. The data necessary for aluminized propellants are commonly obtained by sampling techniques and subsequent particle-size and chemical analyses. The sampling technique,

DOI: 10.13009/EUCASS2019-260

developed in the Institute of Chemical Kinetics and Combustion for aluminized propellants, is described in [16] [24]. In [25], we have adapted and applied it for studying propellants with boron as a single metal fuel in the amount of 12 % to 40 %. Changes in the technique due to the use of boron are presented in [25] along with a list of works in which the condensed combustion products (CCP) of boron-containing propellants have been studied with use of the sampling technique. In [26] [27] the same method was used to study propellants with aluminum diborides, including the mechanically activated ones, and boron carbide. The goal of current work was to compare some previously and first time studied boron-containing fuels.

2. Propellants, components, and fuel characteristics

Formulations of the propellants studied are summarized in Table 1.
A propellant identifier ID contains information on the nominal percentage and the type of metal fuels. Thus, propellant 40B nominally includes 40 % of boron, and propellant 40B4C nominally includes 40 % of boron carbide, etc. The real values may differ a bit from the nominal ones due to the technological peculiarities of the preparation of mixtures.

Table 1: Component composition (% mass) of model propellants

Propellant ID	Binder	B	Al	AlB2	AlB2f	MA3	AlB12	B4C	APf	AP
40B	30.50	37.57							10.33	21.60
40AB	30.50	-	-	37.50					10.67	21.33
40ABF	30.50	-	-		37.50				10.67	21.33
40MA3	30.51					37.49			10.67	21.33
21A17B	31.19	16.54	20.51						10.59	21.17
40AB12	30.50	-	-				37.50		10.67	21.33
6A31B	30.50	6.45	31.05						10.67	21.33
40B4C	30.50	-						37.50	10.67	21.33

The following components were used to produce model propellants:
Binder – active fuel-binder, based on methylpolyvinyl-tetrazole polymer, plasticized by nitro-containing compounds [28].

Metal fuels:
B – amorphous boron [29].

Al – aluminum “ASD-4” [30].

21A17B, 6A31B – a mechanical mixture of Al and B, taken in the same mass ratio as in aluminum diboride and aluminum dodecaboride, respectively, below referred to as “aluminum diboride imitator” and “aluminum dodecaboride imitator”.

AlB2 – aluminum diboride AlB_2, 28 years old [25].

AlB2f – the same aluminum diboride AlB_2 with polymeric fluorine-containing coating called FAOS, 28 years old [25]. A mass fraction of the coating matter was about 4% so that 37.50 % of AlB2f contain 1.5 % of FAOS and 36 % of AlB2.

DOI: 10.13009/EUCASS2019-260

AlB12 – aluminum dodecaboride AlB_{12}, produced by mechanical activation. It is only assumed to be the AlB_{12} compound because the X-Ray phase analysis has failed to verify a corresponding phase composition. One year old.

MA3 – aluminum diboride AlB_2, produced by vacuum annealing of mechanically activated raw material and then again subjected to mechanical activation. It is the most reactive of the three mechanically activated materials, studied in [26], and it is one year old.

The mechanically activated fuel components AlB12 and MA3 were produced in the Institute of Solid State Chemistry and Mechanochemistry, Siberian Branch of the Russian Academy of Sciences (Novosibirsk) using a planetary mill AGO-2 [31] as described in [32] [33].

B4C – boron carbide B_4C.

APf – fine ammonium perchlorate (AP), powder specific surface 5400 cm^2/g.

AP – sieved AP with a particle size of 250-315 micrometers.

Table 2 summarizes the granulometric characteristics of fuel ingredients as moment-based mean diameters D_{mn}.

Table 2: Mean diameters D_{mn} of fuel components

Material	**Mean diameters D_{mn}, μm**				
	D_{10}	D_{20}	D_{30}	D_{43}	D_{53}
B	2.9	3	3	3.2	3.3
AlB2	3.7	4.4	4.5	11.1	14.9
AlB2f	3.0	3.2	3.2	4.8	5.3
MA3	2.7	3.0	3.7	13.1	20.1
21A17B	Not measured				
AlB12	2.2	2.6	3.4	13.7	20.2
6A31B	2.8	3.1	3.5	7.4	9.6
B4C	2.2	2.4	2.6	4.4	5.1

Table 3 presents the values of the reducing number RN, determined by cerimetric method [34]. According to [25] [26], and using the values of masses and the reducing numbers for both initial components and sampled condensed combustion products, one may determine the total incompleteness of fuel combustion without differentiation into components for combined fuels. For details of cerimetric method and of the calculations using its results, see [35] [36].
Table 3 also contains the reference data on the specific heat of the fuels used.

DOI: 10.13009/EUCASS2019-260

Table 3: The values of reducing number RN and specific heat Q for metal fuels

Material	RN	*N*	Theoretical value of RN	Q, kJ/g
Al	10.6±0.2[a]	7[b]	11.1[c]	31.1
B	22.1±0.2	5	27.8	58.9
AlB2	16.1±0.2	3	18.5	43.61
AlB2f	13.6±0.1	3	$18.5\cdot(1-m_{FAOS})$[d]	43.61
21A17B (55.4 % Al + 44.6 % B)	Not measured		15.7	43.499
AlB12	16.6±0.5	3	20.1	52.5
6A31B (17.2 % Al + 82.8 % B)	19.3±0.2	3	20.1	54.118
MA3	14.0±0.1	3	18.5	43.61
B4C	22.3±0.3	4	21.8	49.1

[a]The number after the ± sign is the mean-square deviation Sd.
[b]*N* – the number of definitions.
[c]A theoretical RN value for a mixture is calculated for pure aluminum and boron: $RN(Al+B) = RN(Al)\cdot\omega(Al) + RN(B)\cdot\omega(B) = 11.1\cdot\omega(Al) + 27.8\cdot\omega(B)$, where ω is the mass fraction of the corresponding component in a mixture.
[d]m_{FAOS} – mass fraction of FAOS coating.

3. Experimental technique and conditions. Processing and presentation of results

The experiments were performed at nitrogen pressures of 1.2 MPa and 2.5 MPa by use of the sampling technique [16] [24] followed by cerimetric analysis [34] of sampled CCP as described in [25] [26], and with measuring an average burning rate in each experiment. A morphological analysis of CCP particles was performed using an optical microscope, and in some cases, a scanning electron microscope (SEM) Merlin|VP Compact (Zeiss) with an EDS-device X-Max^N (Oxford Instruments) for local element analysis (EDS – energy dispersive spectroscopy).

The specimens were the non-cured mixtures (Table 1), placed in quartz glasses with a teflon bottom. The inner diameter of the glass (specimen diameter) was 10 mm, and its depth (specimen length) was either five or ten mm. The specimens were ignited with a nichrome wire, using metal-free igniting paste, applied to the specimen surface. The particles were extinguished near the burning surface at a distance of ~25 mm, so that the sampled and studied particles were the so-called primary CCP [23].
The CCP particles were subjected to granulometric and chemical analyses. The results of the particle size analysis were presented in the form of histograms of the size distribution density of the relative mass of CCP particles: $f_i(D) = m_i/(M_{prop}\cdot\Delta D_i)$, where m_i is the mass of CCP in the *i*-th histogram interval, M_{prop} is the mass of propellant (total for all samples burned in series at given conditions), ΔD_i is the width of the *i*-th histogram interval [16] [24]. In some cases we calculated the moment-based mean diameters D_{mn} as the statistical parameters of the function $f(D)$.
In addition, the residues were weighed in a glass after specimen burning-out (the so-called “mass of carcass”). As a result, we obtained the mass size distribution of particles in the range of 0.5 micrometers to millimeters and calculated the below parameters. The mass parameters were scaled with the propellant mass to reduce them to the dimensionless form.
m_{mf} – the dimensionless mass and mf – the mass fraction of metal fuel in the propellant, $m_{mf} \equiv$ mf.
m_{ccp} – the dimensionless CCP mass captured with sampling elements and with the elements of interior of the bomb, exclude the carcass mass.
m_s – the dimensionless carcass mass.
$CCP = m_{ccp} + m_s$ – the total dimensionless CCP mass.
CCPt – the total dimensionless theoretical CCP mass. It is calculated assuming a complete transformation of B into B_2O_3 and of Al into Al_2O_3 with corresponding stoichiometric coefficients by the formula CCPt = <dimensionless boron mass in propellant specimen> × 3.22 + <dimensionless aluminum mass in propellant specimen> ×1.89.

DOI: 10.13009/EUCASS2019-260

CCP / CCPt – the ratio between the really collected CCP mass and its theoretical value. This parameter indirectly characterizes the combustion completeness of metal fuel because the main peculiarity of our sampling technique is almost 100 % efficiency of particle capture.
RN_{mf} – the reducing number of metal fuel.
RN_{mft} – a theoretical value of the reducing number of metal fuel, calculated by an additive formula, see comment ([c]) to Table 3.
RN_{prop} – the reducing number of propellant (the product of RN for the fuel component and its mass fraction in the propellant).
RN_{ccp} – the reducing number of CCP.
$\eta = RN_{ccp} / RN_{prop}$ – the combustion incompleteness of metal fuel.
$E = (1-\eta)\cdot m_{mf}\cdot(RN_{mf} / RN_{mft})\cdot(1-m_s)\cdot Q$ – the energy release efficiency, where Q is the specific heat of fuel combustion, for values see Table 3. The factor$\cdot(RN_{mf} / RN_{mft})\cdot$takes into account the degradation of metal fuel. Note that this expression to determine E differs from that used in [25] [26].

4. Experimental results: burning rate, mass of CCP and combustion incompleteness

The main results are summarized in Table 4 and Figures 1-3.

Table 4: Burning rate, CCP mass parameters, and combustion incompleteness of metal fuel

Propellant ID	*p*, MPa	*r*, mm/s	m_{ccp}	m_s	CCP/CCPt	η
40B	1.2	7±1	0.73±0.02	0.03	0.63±0.02	0.82±0.02
	2.4	8.7±0.5	0.88±0.01	0.05	0.77±0.01	0.70±0.02
40AB	1.2	5.5±0.2	0.38±0.04	0.20±0.02	0.62±0.03	0.70±0.04
	2.2	7.3±0.2	0.39±0.02	0.05±0.01	0.62±0.02	0.70±0.02
40ABF	1.2	8.8±0.6	0.36±0.01	0.24±0.01	0.67±0.01	0.73±0.02
	2.3	9.0±0.3	0.41±0.03	0.19±0.02	0.67±0.01	0.73±0.03
40MA3	1.2	9.3±0.3	0.424±0.001	0.17±0.03	0.64±0.02	0.35±0.01
	2.3	12.1±0.1	0.40±0.01	0.20±0.01	0.65±0.01	0.32±0.01
21A17B	1.2	5.9±0.5	0.30±0.03	0.21±0.01	0.56±0.01	0.62±0.03
	2.2	8.7±0.5	0.45±0.03	0.24±0.01	0.64±0.01	0.61±0.03
40AB12	1.2	6.5±0.3	0.66±0.01	0.028±0.001	0.61±0.01	0.96±0.01
	2.3	10.7±0.2	0.596±0.001	0.07±0.01	0.56±0.01	0.81±0.01
6A31B	1.2	4.3±0.8	0.66±0.02	0.027±0.002	0.61±0.02	0.83±0.02
	2.9	8.7±0.4	0.65±0.03	0.027±0.001	0.60±0.02	0.72±0.03
40B4C	1.1	6.4±0.4	0.54±0.03	0.013±0.002	0.59±0.02	0.76±0.02
	2.3	10.0±0.5	0.54±0.03	0.012±0.001	0.58±0.03	0.76±0.02

The number after the ± sign is the standard error of the mean, Se

Figure 1 demonstrates the data on burning rate. To complete the picture, the point for propellant 40B is plotted along with those for propellants 50B and 24B [25] [26]. Points 50B, 40B, and 24B are connected by straight segments to form a “boron line”.

DOI: 10.13009/EUCASS2019-260

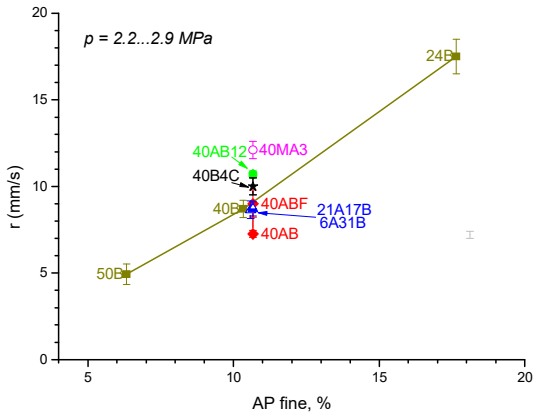

Figure 1: Dependence of burning rate *r* at a pressure of about 2.5 MPa on percentage of fine AP in the propellant.

As follows from Figure 1, the burning rate of propellants with boron only (boron line 50B → 40B → 24B) at a pressure of 2.5 MPa increases almost linearly from 5 to 17 mm/s with increasing fraction of fine AP. When the fixed mass content of fine AP is about 11 % and that of metal fuel is about 40 %, the burning rate varies, depending on fuel nature, from 7.5 to 12 mm/s. The minimal burning rate is recorded for propellant 40AB with old aluminum diboride, and the maximal one corresponds to propellant 40MA3 with fresh, mechanically activated aluminum diboride. It is worth noting that the burning rates of propellants 21A17B and 6A31B with a mechanical mixture of aluminum and boron were close to each other and to those of propellants 40B and 40ABF (~ 9 mm/s) despite the difference in the Al/B ratio. In this case, propellants 40AB12 and 40B4C have a higher burning rate (~10…11 mm/s).

Figure 2 demonstrates the regularities of the change in the dimensionless CCP mass with varying propellant composition.

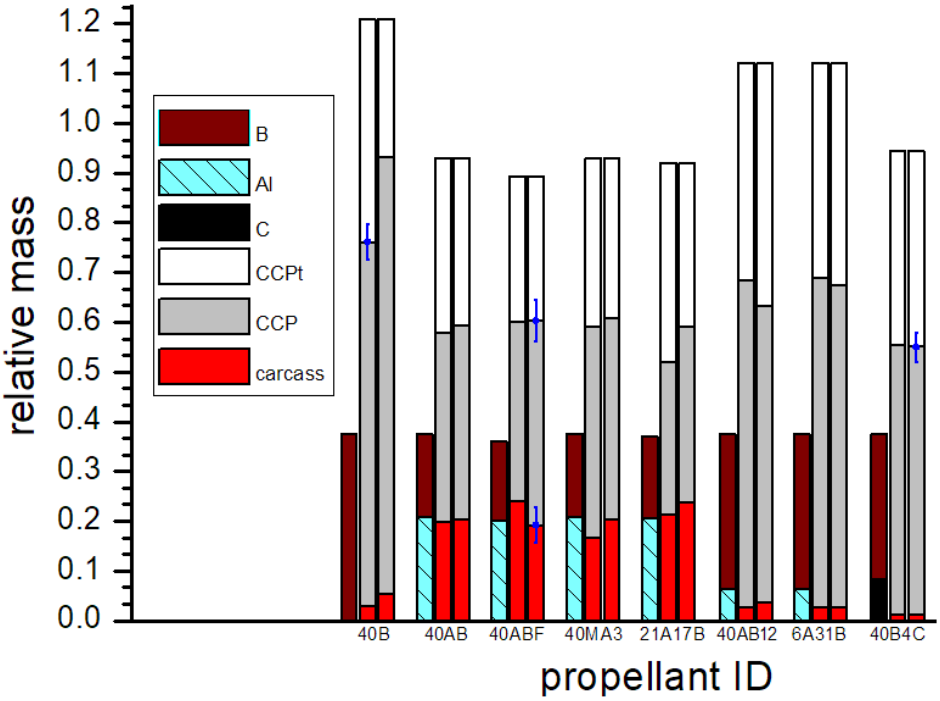

Figure 2: Comparison of CCP mass parameters of the propellants studied

Three bars of mass-proportional heights are constructed for each propellant (their IDs are under the x-axis). The first one shows the content of metal fuel in the propellant. It is one-color for pure boron. In the case of combined fuel, it is

DOI: 10.13009/EUCASS2019-260

two-color and its components are proportional to the masses of boron, aluminum or carbon for propellant 40B4C. The total height of the bar corresponds to the total fuel mass in the propellant. The second and third bars refer to combustion products; the second corresponds to a pressure of 1.2 MPa, and the third one – to a pressure of 2.3 MPa. These bars are three-color. The full height of the colorless bar shows the maximal theoretical CCP mass, CCPt, calculated assuming complete transformations of boron and aluminum into their oxides. The gray CCP bar corresponds to the really collected CCP mass. The CCP mass, remaining in the glass (carcass), is highlighted (the bottom of the gray bar). The confidential intervals in Figure 2, are determined for the reliability level of 68 % by reproducibility test [37]. Not to clutter the picture, the intervals are drawn only at some bars with the worst reproducibility.

The analyses of both Figure 2 and the data of Table 4 indicate the following.

- The increase in pressure 1.2 MPa → 2.3 MPa has a weak effect on the CCP mass but leads to the increase in carcass mass. It can be attributed to the decrease in the velocity of the gaseous products flowing from the burning surface at the changing of pressure and burning rate. The variation in both the CCP mass and the carcass mass with pressure are not large and in most cases, within the error limits.
- The presence of aluminum in the combined fuel of the aluminum diboride type causes the increase in carcass mass which is readily observed by comparing propellants 40B and the group of diboride propellants (40AB, 40ABF, 40MA3, 21A17B). At the same time, the carcass mass in the group of the aluminum dodecaboride type propellants (40AB12, 6A31B) is comparable with that for propellant 40B.
- Propellant 40B4C has the smallest carcass mass among those compared in this work.

Thus, the main factors, affecting the carcass mass, are the burning rate and the type of metal fuel. The presence of aluminum strengthens the tendency of fuel to carcass formation.

Figure 3 shows the value of energy release efficiency, E, for the propellants studied at both pressures. To prevent cluttering the figure, only the three largest confidential intervals are shown. The error depends mainly on the accuracy of the experimental determination of combustion incompleteness. A horizontal dotted line corresponds to propellant 40B4C.

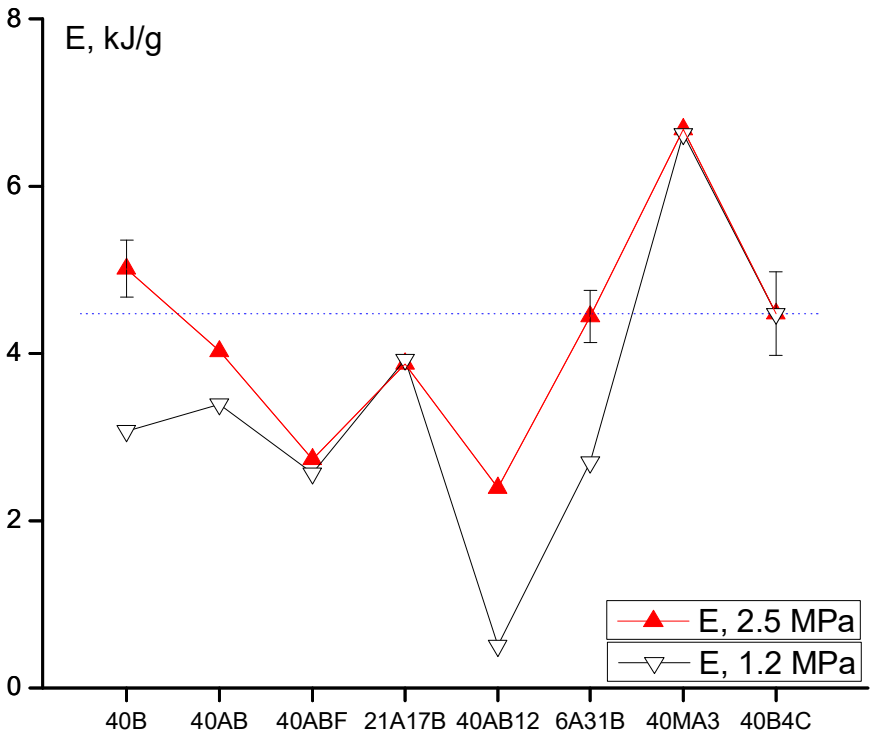

Figure 3: Energy release efficiency, E, for the propellants under study. Comparison at two pressure levels

The analysis of Figures 2, 3 and of Table 4 indicates the following.

DOI: 10.13009/EUCASS2019-260

- Parameter E for the “aluminum diboride group” propellants (40AB, 40ABF, 21A17B, 40MA3) can *in principle* exceed that for the propellant 40B with boron only (e. g., propellant 40MA3) despite the increase in carcass mass. For propellant 40MA3, this is reached by decreasing combustion incompleteness due to the increase in fuel reactivity via mechanical activation.
- The propellants of the aluminum dodecaboride group (40AB12, 6A31B) exhibit no advantages over the propellants of the aluminum diboride group and propellant 40B despite the smaller carcass mass. It is assumed, however, that the studies on the formulations with aluminum diboride should be continued using material of higher phase purity.
- Although propellant 40B4C has a smaller carcass mass, it is comparable with propellants 6A31B and 40B in parameter E. It is assumed then that the studies on the formulations with boron carbide should also be continued.
- The key factor which defines the energy release efficiency, E, is the combustion incompleteness η. This is due to the fact that the value of η varies within the wide range 0.32…0.96, whereas the parameter of dimensionless carcass mass, m_s, varies from 0.01 to 0.24 for the set of propellants studied.

5. Experimental results: morphology of the combustion product particles

The morphology of the combustion product for the propellants containing single boron as metallic fuel was described in [25]. Briefly, it has been established that in this case the CCP are composed mainly of agglomerated boron and boron oxide B_2O_3\H_3BO_3. Oxide white residue represents the aggregates consisting of submicron particles. The boron agglomerates are dark and have either the teardrop or spherical shape which testifies to the partial melting of boron. The size of agglomerates exceeds the particle size of initial boron by order of magnitude.
In this chapter the CCP particle morphology is described for the combined fuel containing Al and B. The fuel MA3 provides an excellent example of the aluminum diboride type of combined fuel. The fuel MA3 is “double mechanically activated” [26]. As it follows from data of Table 4 and Figures 1, 2, the propellant 40MA3 is characterized by highest burning rate, rather low incompleteness of combustion, and relatively high carcass mass.
In general, the presence of aluminum in the combined fuel intensifies the agglomeration which, in turn, caused the increase in the size of CCP particles and in carcass mass (residues in the glass). Both in the sampled CCP and in the carcass mass there are large baked sintered agglomerate particles of irregular shape. In addition there are coarse spherical particles in the CCP similar to “classical” aluminum agglomerates [38], especially in the cases of mechanically activated diboride fuels. We extracted these particles and subjected to particle size, morphology and SEM\EDS analyses. The typical results are presented in Figure 4–6 and in Table 5. Figure 4 shows the size distribution density of the relative mass of the spherical CCP particles. The plots are normalized so that the area under curves equals 1. Remember that spherical particles present only part of the whole CCP collection, but the important part. Typically, there is correlation of the particle size and the combustion incompleteness. As follows from Figure 4 and Table 5, the size of the particles reaches the hundreds of micrometers. It is of interest to examine the morphology of spherical particles.

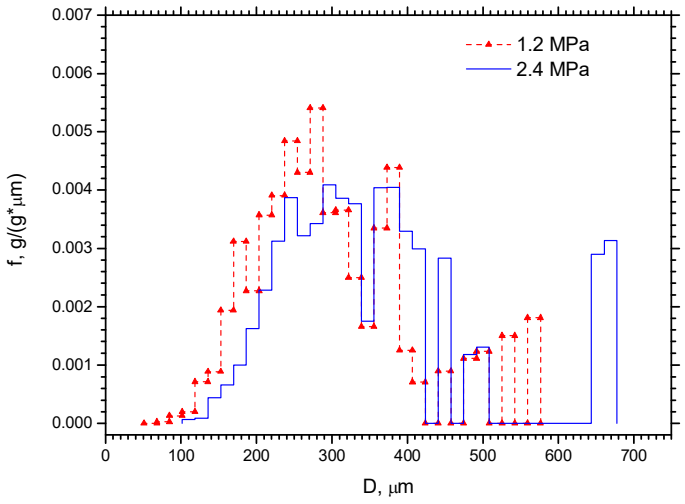

Figure 4: Normalized mass size distribution functions for spherical CCP particles of the 40MA3 propellant at two pressure levels.

DOI: 10.13009/EUCASS2019-260

Table 5: Mean diameters D_{mn} of the spherical CCP-particles for the 40MA3 propellant

Pressure, MPa	**Mean diameters[a] D_{mn}, μm**					***N***
	D_{10}	D_{20}	D_{30}	D_{43}	D_{53}	
1.2	209	233	237	301	318	450[b]
2.3	252	266	283	356	379	253[b]

[a]The values of D_{mn} reported as calculated (not rounded). Unstrumental error is ±9 μm
[b]N is the number of particles measured

Figures 5–6 illustrate the morphology and the results of SEM\EDS analyses of spherical CCP particles. In the first case, Figure 5, the analysis was performed with the point on the outer surface of particle, and boron was not found on the particle surface. In the second case, Figure 6, the analysis was performed with the area inside the particles. For this end several particles were subjected to of mechanical "lancing". The EDS analysis was performed with area (not a point). It has been established that spherical particles have structure of *nucleus-in-shell*. Despite that the boron was not found on the particle surface, it is presented in the interior of particle in large quantity (for example, in case of propellant 40MA3 in the nucleus material there are more than 80 at. % of B). It is interesting to note that similar morphology has been registered in [39] [40] for model agglomerates with a diameter of 320-780 micrometer formed of the combined fuel with Al/B = 4.23/1, burning in air at 0.1 MPa.

DOI: 10.13009/EUCASS2019-260

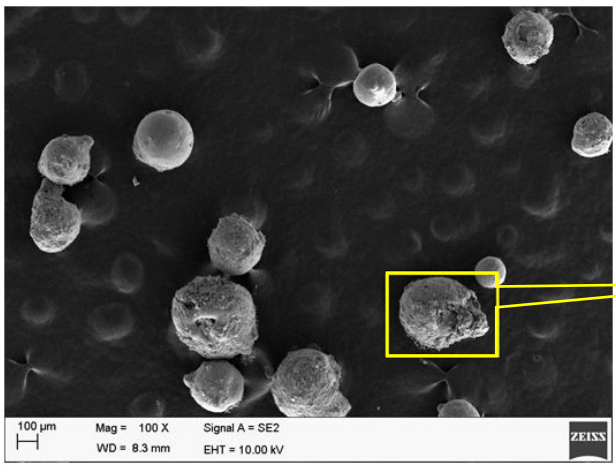

a)

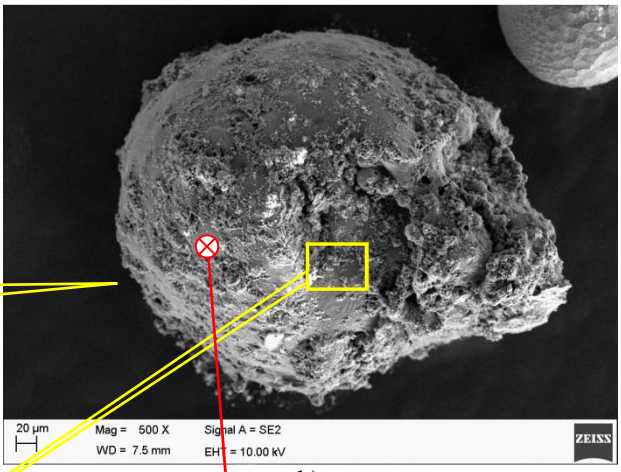

b)

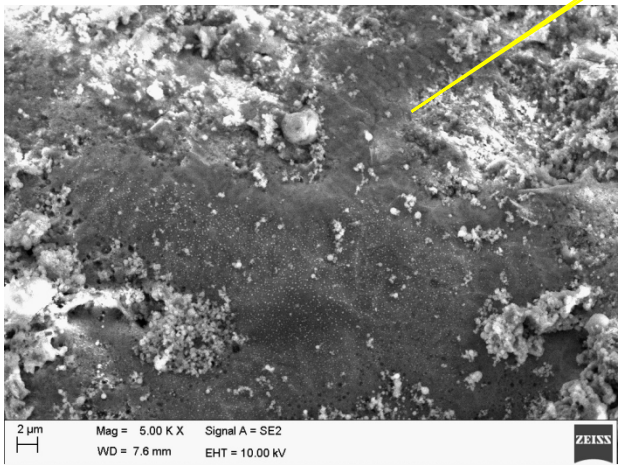

c)

EDS data on the local content of chemical elements

Element	Weight %	Atomic %
C	42.46	51.61
O	46.46	42.39
Al	11.07	5.99

d)

Figure 5: Propellant 40MA3, spherical CCP particles sampled at pressure 2.3 MPa.
(a), (b), (c) – the SEM-images at various magnification, (d) – the results of SEM\EDS analysis in one random point **at the surface** of a spherical particle. Point of analysis is labeled in the picture (b) with sign ⊗.

DOI: 10.13009/EUCASS2019-260

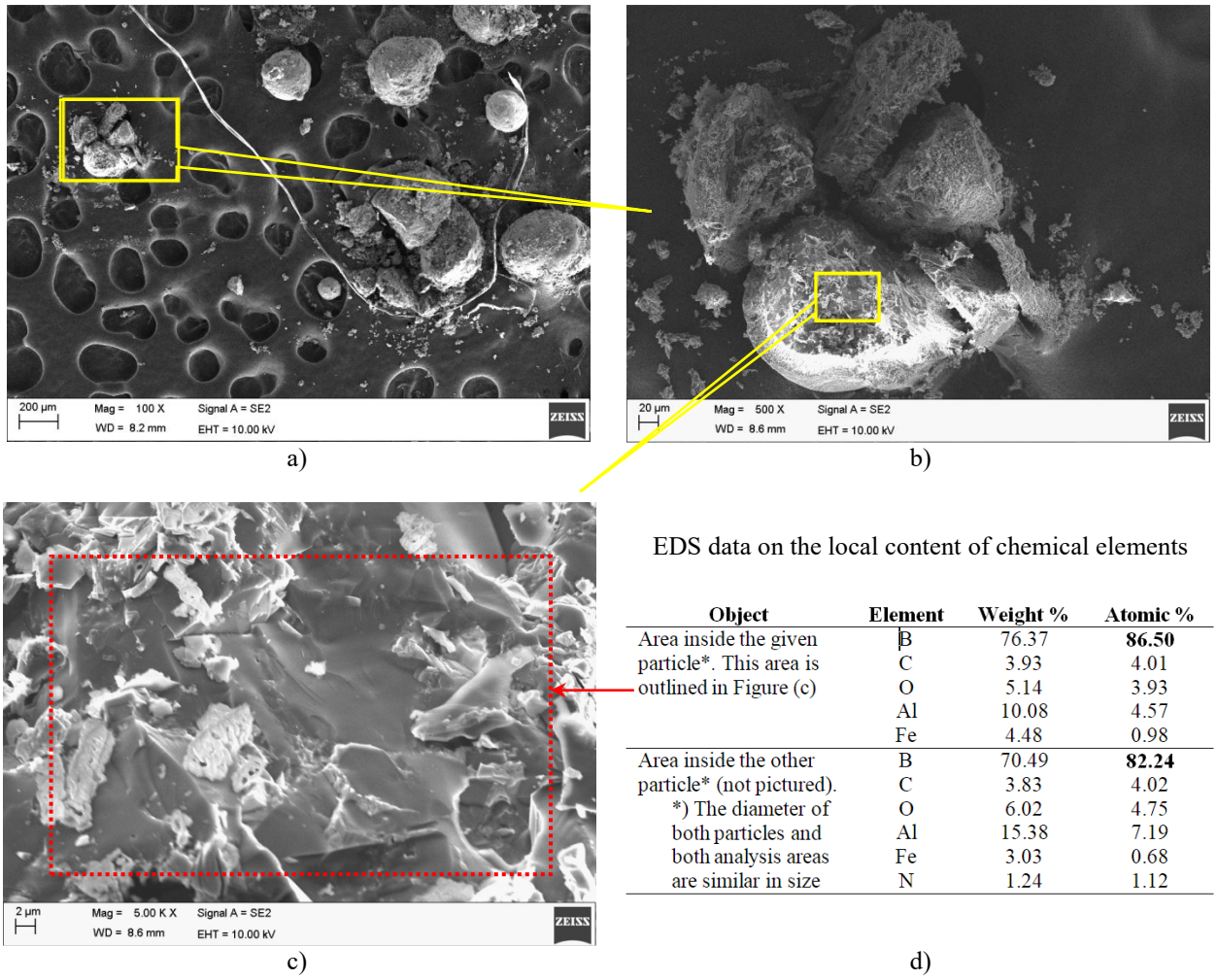

EDS data on the local content of chemical elements

Object	Element	Weight %	Atomic %
Area inside the given particle*. This area is outlined in Figure (c)	B	76.37	**86.50**
	C	3.93	4.01
	O	5.14	3.93
	Al	10.08	4.57
	Fe	4.48	0.98
Area inside the other particle* (not pictured). *) The diameter of both particles and both analysis areas are similar in size	B	70.49	**82.24**
	C	3.83	4.02
	O	6.02	4.75
	Al	15.38	7.19
	Fe	3.03	0.68
	N	1.24	1.12

d)

Figure 6: Propellant 40MA3, spherical CCP particles sampled at pressure 2.3 MPa.
One of the particles has been destroyed with sharp scalpel.
(a), (b), (c) – the SEM-images at various magnification, (d) – the results of SEM\EDS analysis by the area **inside** the particle. Area of analysis is labeled in the picture (c) with rectangle ▭

It was assumed in [26] that in this case mechanical activation has led to deeper oxidation of metal fuel in the condensed phase. According to the literature data, it is the factor promoting agglomeration both in case of the aluminized propellants [41], and in case of propellants with boron additive [16]. Oxidation of metal leads to accumulation of oxide that makes stronger the holding force for agglomerates on the burning surface.

6. Conclusions

New experimental information is obtained on the burning rates and the characteristics of condensed combustion products of heavy-loaded composite propellants with boron-containing fuels. In the case of presence in the system of aluminum in the form of an individual component or as a part of the aluminum diboride or dodecaboride, the spherical particles may appear in CCP. These particles have structure of nucleus-in-shell and boron is concentrated in nucleus. The propellants studied are ranged by the energy release efficiency parameter, which integrates such factors as fuel combustion incompleteness, a fuel mass fraction in propellants, the reducing number of fuel, the amount of residue in a glass, and the specific heat of fuel combustion. The data obtained indicate that the studies on the propellants with the activated aluminum diboride as well as the formulations with boron carbide seem rather promising.

Acknowledgements

The work was supported by the Russian Foundation for Basic Research (project 15-03-04321). The authors are grateful to Fedotova T. D. and Nesterenko L. N. for performing chemical analyses and Korchagin M. A. for production of the mechanically activated materials.

References

[1] Sarner S.F. 1966. Propellant Chemistry. N. Y.: Reinhold Publishing Corporation.
[2] Pokhil P.F., Belyayev A.F., Frolov Y.V., Logachev V.S., Korotkov A.I. 1972. Combustion of Powdered Metals in Active Media. Moscow: Nauka, [in Russian].
[3] Yagodnikov D.A. 2009. Ignition and combustion of powdered metals. Moscow: The Bauman Moscow State Tecnical University Publishing House. [in Russian]
[4] Kuo KK, Pein R, editors. 1993. Combustion of Boron-based Solid Propellants and Solid Fuels. Boca Raton: CRC Press.
[5] Pang W., De Luca L.T., Fan X., Glotov O.G., Zhao F. 2019. Boron-Based Fuel-Rich Propellant: Properties, Combustion, and Technology Aspects. CRC Press, Taylor & Francis Group, an Informa Group company,
[6] Meerov D., Monogarov K., Bragin A., Frolov Y., Nikiforova A. 2015. Boron Particles Agglomeration and Slag Formation During Combustion of Energetic Condensed Systems // *Physics Procedia*, Vol. 72, pp. 85-88, https://doi.org/10.1016/j.phpro.2015.09.024.
[7] Pang.W., Fan X., Zhao F., et al. 2013. Effects of Different Metal Fuels on the Characteristics for HTPB-based Fuel Rich Solid Propellants // *Propellants, Explosives, Pyrotechnics*, Vol. 38, pp. 852-859.
[8] Yagodnikov D.A. 2010. Experimental Study of Combustion of a Cloud of Boron Particles in Air // Combustion, *Explosion, and Shock Waves*, Vol. 46, No. 4, pp. 426–432.
[9] Il'in A.P., Gromov A.A. 2002. Combustion of ultra-fine aluminum and boron. Tomsk: Tomsk State University Publ. [in Russian]
[10] Gromov A.A., Habas T.A., Il'in A.P., Popenko E.M., Korotkikh A.G., Arkhipov V.A., Ditz A.A., Strokova Y.I., Tolbanova L.O. 2008. Combustion of nano-sized metal powders. Tomsk: Deltaplan Press, [in Russian]
[11] Yu J. Combustion behaviors and flame microstructures of micro- and nano-titanium dust explosions, 2016. *Fuel*, Vol. 181pp. 785–792.
[12] Calabro M. 2009. Overview on Hybrid Propulsion // Eucass 2009, 3rd European conference for aero-space sciences, France, Paris, July 6-9, Proceedings on CD.
[13] DeLuca L.T., Galfett I.L., Severini F., Rossettin I.L., Meda L., Marra G., D'Andrea B., Weiser V., Calabro M., Vorozhtsov A.B., Glazunov A.A., Pavlovets G.J. 2007. Physical and Ballistic Characterization of AlH_3-based Space Propellants // *Aerospace Science and Technology*, Vol. 11, No. 1, pp. 1-8.
[14] Glotov O.G., Zarko V.E., Beckstead M.W. 2000. Agglomerate and Oxide Particles Generated in Combustion of Alex Containing Solid Propellants // Energetic materials. 31th Int. Annual Conf of ICT. Karlsruhe, Germany. pp. 130-1–130-14.
[15] Gao W., Zhanga X., Zhang D., Peng Q., Zhang Q., Dobashi R. 2017. Flame propagation behaviours in nano-metal dust explosions // *Powder Technology*, Vol. 321, pp. 154–162.
[16] Korotkikh A.G., Glotov O.G., Arkhipov V.A., Zarko V.E., Kiskin A.B. 2017. Effect of iron and boron ultrafine powders on combustion of aluminized solid propellants // *Combustion and Flame*, Vol. 178, pp. 195-204.
[17] Gany A., Timnat Y.M. 1993. Advantages and drawbacks of boron-fueled propulsion // *Acta Astronautica*, Vol. 29, No. 3, pp. 181-187.
[18] Alexandrov V.N., Bytskevich V.M., Verkholomov V.K., Gramenitsky M.D., Dulepov N.P., Skibin V.A., Surikov E.V., Hilkevich V.Y., Yanovsky L.S. 2006. Integrated ramjet engines on solid propellants (Bases of the theory and calculation). Moscow: Akademkniga, [in Russian]
[19] Sorokin V.A., Yanovsky L.S., Kozlov V.A., Surikov E.V., Sharov M.S., Feldman V.D., Frantsevicg V.P., Zhivotov N.P., Abashev V.M., Chervakov V.V. 2010. Rocket ram jet motors on solid and pastelike propellants. Moscow: Fizmatlit. [in Russian].
[20] Maček A., Semple J.M. 1970. Combustion of boron carbide, Final report on Contract N00123-69-C-2365.
[21] Yagodnikov D.A., Voronetskii A.V., Sarab'ev V.I. 2016. Ignition and combustion of pyrotechnic compositions based on micro- and nanoparticles of aluminum diboride in air flow in a two-zone combustion chamber // *Combustion, Explosion, and Shock Waves*, Vol. 52, No. 3, pp. 200-306.

[22] Rashkovskii S.A., Milekhin Y.M., Fedorychev A.V. 2017. Effect of distributed injection of air into the afterburning chamber of a ram-rocket engine on the efficiency of combustion of boron particles // *Combustion, Explosion, and Shock Waves*, Vol. 53, No. 6, pp. 652–664.

[23] Liu J., Liang D., Xiao J., Chen B., Zhang Y., Zhou J., Cen K. 2017.Composition and characteristics of primary combustion products of boron-based propellants // *Combustion, Explosion, and Shock Waves*, Vol. 53, No. 1, pp. 55–64.

[24] Glotov O.G., Zyryanov V.Y. 1995. Condensed combustion products of aluminized propellants. I. A technique for investigating the evolution of disperse-phase particles // *Combustion, Explosion and Shock Waves*, Vol. 31, No. 1, pp. 72-78.

[25] Glotov O.G., Zarko V.E., Surodin G.S., Kiskin A.B. 2017. Combustion efficiency of boron containing fuels in composite propellants // Energetic Materials. Reactivity and Modeling. 48th International Annual Conference of the Fraunhofer Institute for Chemical Technology (ICT). Karlsruhe, Germany, June 27 – 30, 2017. pp. 14-1–14-14.

[26] Glotov O.G., Surodin G.S., Zarko V.E., Korchagin M.A. 2018. Combustion characteristics of model composite propellants with aluminum diboride // Energetic Materials. Synthesis, Processing, Performance. 49th Int. Annual Conf. of ICT. Karlsruhe, Germany, June 26 – 29, 2018. pp. 110-1–110-14.

[27] Glotov O.G., Surodin G.S., Ermolaev G.V. 2019. Combustion characteristics of model composite propellants with boron carbide // Energetic Materials – Past, Present and Future. 50th International Annual Conference of the Fraunhofer ICT. June 25 – 28, 2019. Karlsruhe, Germany. pp. 80-1-80-13.

[28] Arkhipov V.A., Gorbenko T.I., Zhukov A.S., Pesterev A.V. 2011. Tin Chloride Effect on the Burning Rate of the Heterogeneous Condensed Systems // *Chemical physics and mesoscopy*, Vol. 13, No. 4, pp. 463–469. [in Russian]

[29] Oxygen-free compounds of boron: catalog of products of the enterprise and their technical characteristics. – Yekaterinburg, UniHim with a pilot-production plant, JSC. // http://www.unichim.com/docum/catalogs/. URL: https://yadi.sk/i/Dyu4fdL83RmPC2 (access date: 08.06.2019). [in Russian]

[30] Yagodnikov D.A., Gusachenko E.I. 2004. Experimental Study of the Disperse Composition of Condensed Products of Aluminum-Particle Combustion in Air // *Combustion, Explosion and Shock Waves*, Vol. 40, No. 2, pp. 154–162.

[31] Mills and mechanochemical activators: [site]. 2019. URL: http://www.solid.nsc.ru/en/developments/equipments/mills-and-mechanochemical-activators/ (access date: 13.1.2019).

[32] Korchagin M.A., Zarko V.E., Bulina N.V. 2017. Synthesis of Nanocrystalline Magnesium and Aluminum Diborides // *Eurasian Chemico-Technological Journal*, Vol. 19, No. 3, pp. 223-229.

[33] Korchagin M.A., Gavrilov A.I., Bokhonov B.B., Bulina N.V., Zarko V.E. 2018. Synthesis of Aluminum Diboride by Thermal Explosion in Mechanically Activated Mixtures of Initial Reagents // *Combustion, Explosion, and Shock Waves*, Vol. 54, No. 4, pp. 424–432.

[34] Fedotova T.D., Glotov O.G., Zarko V.E. 2007. Application of Cerimetric Methods for Determining the Metallic Aluminum Content in Ultrafine Aluminum Powders // *Propellants, Explosives, Pyrotechnics*, Vol. 32, No. 2, pp. 160–164.

[35] Glotov O.G., Simonenko V.N., Zarko V.E., Tukhtaev R.K., Grigor'yeva T.F., Fedotova T.D. 2004. Combustion characteristics of propellants containing aluminum-boron mechanical alloy // Energetic materials. Structure and properties. 35th Int. Ann. Conf. of ICT. Karlsruhe, Germany. pp. 107-1–107-18.

[36] Glotov O.G., Zarko V.E., Simonenko V.N., Fedotova T.D., Tukhtaev R.K., Grigor'yeva T.F. 2005. Effect of Al/B mechanical alloy on combustion characteristics of AP/HMX/energetic binder propellants // Energetic Materials. Performance and Safety. 36th Int. Ann. Conf. of ICT & 32nd Int. Pyrotech. Seminar. Karlsruhe, Germany. pp. 102-1–102-12.

[37] Glotov O.G. 2000. Condensed combustion products of aluminized propellants. II. Evolution of Particles with Distance from the Burning Surface // *Combustion, Explosion, and Shock Waves*, Vol. 36, No. 4, pp. 476-487.

[38] Zarko V.E., Glotov O.G. 2013. Formation of Al oxide particles in combustion of aluminized condensed systems (Review) // *Science and Technology of Energetic Materials*, Vol. 74, No. 6, pp. 139-143.

[39] Glotov O.G., Surodin G.S. 2019. Combustion of Aluminum and Boron Agglomerates Free Falling in Air. I. Experimental Approach // *Combustion, Explosion, and Shock Waves*, Vol. 55, No. 3, pp. 335–344.

[40] Glotov O.G., Surodin G.S. 2019. Combustion of Aluminum and Boron Agglomerates Free Falling in Air. II. Experimental Results // *Combustion, Explosion, and Shock Waves*, Vol. 55, No. 3, pp. 345–352.

[41] Glotov O.G. 2006. Condensed Combustion Products of Aluminized Propellants. IV. Effect of the Nature of Nitramines on Aluminum Agglomeration and Combustion Efficiency // *Combustion, Explosion, and Shock Waves*, Vol. 42, No. 4, pp. 436-449.